A Photoactivatable Version of Ivabradine Enables Light Induced Block of HCN Current *in vivo*

Alessandro Porro,[1] Edoardo Armano,[2] Federico Brandalise,[1] Rebecca Appiani,[2] Monica Beltrame,[1] Andrea Saponaro,[3] Clelia Dallanoce,[2] Koichi Nakajo,[4] Kaei Ryu,[4] Roberta Leone,[1] Gerhard Thiel,[5] Marco Pallavicini,[2] Anna Moroni,[1] and Cristiano Bolchi [2*]*

[1] Department of Biosciences, University of Milan, Milano, Italy

[2] Department of Pharmaceutical Sciences, University of Milan, Milano, Italy

[3] Department of Pharmacological and Biomolecular Sciences, University of Milan, Milano, Italy

[4] Division of Integrative Physiology, Department of Physiology, Jichi Medical University, Kawachi District, Japan

[5] Department of Biology, TU-Darmstadt, Darmstadt, Germany

Abstract

Therapeutic drugs, whose bioactivity is hindered by a photoremovable cage, allow spatiotemporal confinement of the action to the target diseased tissue with improved bioavailability and efficacy. Here, we have applied such an approach to ivabradine (IVA), a bradycardic agent indicated for angina pectoris and heart failure, acting as a specific HCN channel blocker. To overcome the side effects due to its poor discrimination among HCN channel subtypes (HCN1-4), IVA was linked to a photocleavable bromo-quinolinylmethyl group (BHQ-IVA). Upon illumination with blue light (440

nm), BHQ-IVA releases active IVA that blocks HCN channels currents *in vitro* and exerts bradycardic effect *in vivo*. Both BHQ-IVA and the cage are inactive. Caging is stable in aqueous medium and in the dark and it does not impair aqueous solubility and cell permeation, indispensable for IVA activity. This approach allows to bypass the poor subtype-specificity of IVA expanding its prescription to HCN-related diseases besides cardiac.

KEYWORDS. Ivabradine, HCN channel, Photoactivation, Photocleavable protecting group.

Introduction

Hyperpolarization-activated cyclic nucleotide-gated (HCN) channels conduct the cationic mixed (Na^+ and K^+) current I_f/I_h that controls excitability of cardiac and neuronal cells.[1] HCN channels belong to the superfamily of voltage-gated potassium (Kv) channels. Like Kv channels the functional channel is a tetramer in which the monomers are built of six transmembrane (TM) domains (S1-S6) including the voltage sensor domain (S1-S4) and the pore domain (S5-S6). Typical of HCN channels is their "inverted" voltage-dependency meaning that they activate different from Kv channels at hyperpolarized potentials. This voltage dependency is further modulated by the second messenger cAMP that binds to the cytosolic cyclic nucleotide binding domain (CNBD) of the channel. There are four subtypes in humans, HCN1-4, differentially expressed throughout the body. HCN1 and HCN2 are the main neuronal subtype, expressed in the central and peripheral nervous system, while HCN4 is considered the cardiac subtype, preferentially expressed in the heart pacemaker region, the sinoatrial node. The HCN3 subtype is from a functional point of view less characterized than the others; it is not preferentially expressed in any district tissue, but it is uniformly distributed throughout the body.

HCN channels control crucial physiological functions, from heart rate to neuronal excitability, and their dysregulation is associated with severe human pathologies. This includes life-threatening

cardiac dysfunctions HCN4-related as well as epilepsy and neurodegenerative diseases HCN1 and HCN2-related.[2,3] Recently identified selective and brain-penetrant HCN1 inhibitors have revealed the precise role of HCN1 channels and their potential as a target for the treatment of cognitive dysfunction.[4] HCN2 channels have also gained much attention as a key determinant of nociceptive excitability and in the development of chronic neuropathic pain.[5,6]

Ivabradine (Chart 1) is a blocker highly specific for HCN channels and as such used as a research tool for probing the therapeutic potential of HCN blockade. In the clinics, it is successfully employed specifically as a bradycardic agent with the indication of stable angina pectoris and heart failure treatment.[7,8] But, since ivabradine discriminates only poorly among HCN subtypes,[9] it cannot be used to treat diseases involving HCN channels in other tissues than the heart without risk of negative side effects on heart rate.

The development of subtype-specific ivabradine analogues is challenging because of the high degree of conservation of the ivabradine binding site in all HCN subtypes. This circumstance was recently underlined by a structural study of HCN4 in complex with the drug.[10] For this reason, it is not surprising that previous structural modifications of the ivabradine molecule failed to achieve significant subtype selectivity.[11,12]

If a drug molecule cannot be made target-specific, specificity can then be achieved by delivering the drug to the target tissue only. This could be achieved by derivatizing the bioactive molecule with a photocleavable-protecting group (PPG). In the ideal case, this chemical caging makes the drug molecule inactive until the PPG is cleaved locally in a tissue-specific manner. The use of light to release the drug further ensures a high spatio-temporal resolution. [13,14] A prerequisite for a future medical application is that uncaging from PPG must occur efficiently at biologically compatible wavelengths. Furthermore, good uncaging efficiency, oxygen-independent uncaging mechanism, nontoxicity, proper solubility, cell permeability and metabolic stability are desired properties of a photocaged drug. Indeed, a multitude of parameters need to be balanced in the development a photocage to match the criteria for clinical translation, as-yet unrealized, of this “prodrug” approach.[15]

Developing a light-sensitive caged version of ivabradine, which is a tertiary amine, is confronted with the absence of functional groups such as COOH, OH, SH, and NH that are easy to be caged.[16,17] In the few examples of caged tertiary amines reported in the literature, PPG is covalently attached to nitrogen to form quaternary ammonium salts.[18-21] Compared to standard strategies derivatizing the above functional groups generally to photolabile esters or carbamates, caging by nitrogen quaternarization has the advantage that the aqueous solubility of the bioactive molecule, due to the presence of the fixed positive charge, is increased or, at least, not drastically decreased and its covalent bond with the cage is stable to hydrolysis. Indeed, the examples of bioactive tertiary amines, such as nicotine and tamoxifen, caged by quaternarization and photoactivated in biological experiments show that the presence of a tertiary amine nitrogen as the only cageable function can be a resource rather than a handicap.[19,22] Furthermore, it is reasonable to expect that caging of amine nitrogen by quaternarization hinders the bioactivity of ivabradine, given the importance of the presence of a protonatable nitrogen as suggested by the fact that both ivabradine and its *N*-desmethyl metabolite have bradycardic effect.[23]

We applied this strategy to develop a photoactivatable ivabradine. Among the reported examples of tertiary amines caged by nitrogen quaternarization with a coumarin-4-methyl-,[18] *o*-nitrobenzyl-,[19] *p*-hydroxyphenacyl-[20] or 2-quinolinylmethyl-based[21] alkylating molecule, we chose this latter option considering both the reported photorelease rapidity and wavelengths of uncaging irradiation. The tertiary amine nitrogen was thus quaternarized with 8-bromo-7-hydroxy-2-quinolinylmethyl (BHQ) as a PPG [24,25] to give BHQ-protected ivabradine (BHQ-IVA) (mesylate **1a** and hydroxide **1b**) (Chart 1) preferring BHQ, as-yet unused to photocage bioactive tertiary amines, to CyHQ, its 8-cyano analogue, already successfully experimented in tertiary amines photoactivation, but not so synthetically accessible. This should enable a light-induced release of ivabradine by removal of 8-bromo-7-hydroxy-2-hydroxymethylquinoline (BHQ-OH) (Chart 1). In the long term, this should pave the way for therapeutic inhibition of HCN activity in target cells without undesired side effects thanks to a localized release of the drug.

In this work, we report the synthesis and the photophysical properties of BHQ-protected ivabradine, its photoactivation under different irradiation conditions and its ability to inhibit HCN activity in cells, brain tissues and living organisms.

Chart 1. Bromo-hydroxy-quinolinylmethyl photocleavable protecting group (BHQ-PPG), 8-bromo-7-hydroxy-2-hydroxymethylquinoline (BHQ-OH) resulting from the photocleavage of caged ivabradine, BHQ-protected ivabradine (BHQ-IVA: mesylate (**1a**) or hydroxide (**1b**)) and ivabradine (IVA).

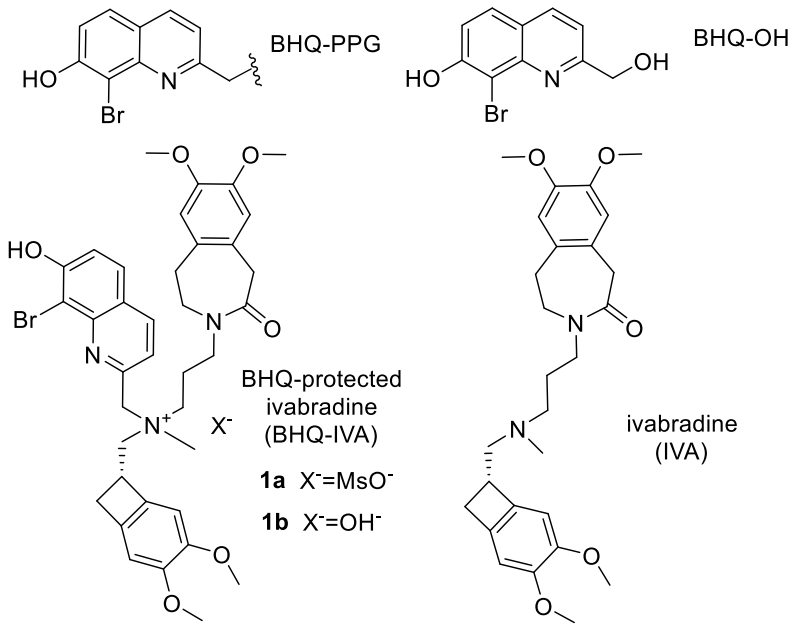

Results and discussion

Synthesis of photocaged Ivabradine

Coupling of commercially available ivabradine with BHQ-OMs (7) gave BHQ-IVA, which was isolated as mesylate (**1a**) or hydroxide (**1b**) (Scheme 1). BHQ-OMs was in turn synthesized in five

steps from 2-methyl-8-bromo-quinolin-7-ol *p*-TSA salt (**2**)[21] according to the general procedures of Dore et al. [21,26,27] with modifications: MOM protection of phenol (**3**), oxidation of the methyl group to formyl (**4**), reduction to hydroxymethyl (**5**), mesylation of the alcoholic function (**6**), and deprotection of phenol (**7**) (Scheme 1).

Scheme 1. Synthesis of BHQ-protected ivabradine (1)[a]

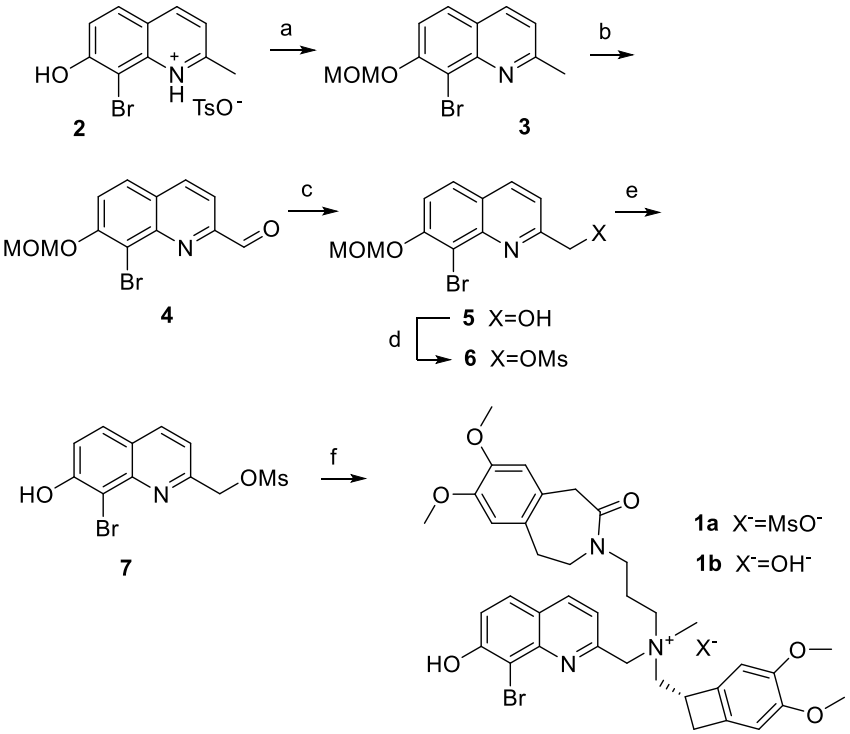

[a] Reagents and conditions: (a) DIPEA, DCM, rt, 30 min, then MOMBr, 0 °C and rt, 16 h, 61%; (b) SeO_2, 1,4-dioxane, 80 °C, 1 h, 100%; (c) NaBH4, EtOH, rt, 1 h, 85%; (d) MsCl, TEA, DCM, 0 °C, 1 h, 67%; (e) TFA, DCM, rt, 8 h, 90%; (f) Ivabradine, CH_3CN, reflux, 3 h, and then flash chromatography eluting with DCM/MeOH (**1a**) or DCM/MeOH/NH_3 (**1b**), 39% and 71% respectively.

Photophysical Properties and Photochemistry

BHQ-protected ivabradine **1a** and **1b** exhibited good solubility (0.55 and 0.43 mM respectively) in the HEPES buffer (pH 7.4) used to simulate physiological conditions in the photochemistry experiments. Their UV-vis spectra recorded in the HEPES buffer showed a λ_{max} at 381 nm (Figure S1). The molar absorptivities at 365, 395 and 440 nm, calculated using the Beer-Lambert law, are reported in Table 1. At room temperature and under simulated physiological conditions (HEPES buffer pH 7.4), less than 1% of **1a** and **1b** degraded during a period of 1 week in the dark or in 20 minutes upon irradiation with 550 nm light. Upon exposure to 365 nm, 395 nm and 440 nm light, **1a** and **1b** released IVA with chemical yields ranging between 44% and 51% (Table 1). The time course of the photolysis reaction was monitored by HPLC, quantifying the disappearance of **1a** and **1b** by comparison with the area of their peaks before irradiation and the appearance of the released IVA using a previously constructed calibration curve (Figure 1). The irradiation times required for 90% of initial **1a** or **1b** to be consumed and the quantum efficiencies (Q_u) at the three wavelengths are reported in Table 1. The chemical yields of released IVA were similar to those reported for a variety of BHQ caged compounds, such as phenols, diols and carboxylates,[25] and CyHQ caged tertiary amines.[21] The yields of released IVA could be lowered by undesired photoreactions of **1a** and **1b**, such as debromination, described to impair the photoactivation of other BHQ caged compounds.[26,28] However, such a reaction should be disadvantaged by the hydrolytic stability of **1a** and **1b** and the good leaving group character of IVA, imputable to its pK_a lower than the established upper threshold for leaving ability (10.1).[28] More likely, as suggested by the progressive appearance of minority peaks eluted just before IVA in the HPLC chromatograms registered during the photolysis, IVA forms secondary photoproducts.[29]

TABLE 1. Photophysical and Photochemical Data for the Photolysis of 1a and 1b[a]

compound	wavelength (nm)	ε ($M^{-1}cm^{-1}$)	I[b] (Einstein $cm^{-2}s^{-1}$)	$t_{90\%}$ (s)	Q_u	Yield[c] (%)
1a	365	2670	0.97×10^{-7}	42.3	0.091	45
	395	2455	1.07×10^{-7}	91.4	0.041	50
	440	217	1.01×10^{-7}	895.3	0.051	51
1b	365	2708	0.97×10^{-7}	51.9	0.073	48
	395	2750	1.07×10^{-7}	98.7	0.034	48
	440	214	1.01×10^{-7}	741.2	0.062	44

[a] 1.5 mM solution in 85:7.5:7.5 HEPES buffer (pH = 7.4):water:DMSO. [b] Intensity of the lamp measured by ferrioxalate actinometry. [c] Chemical yield of released ivabradine.

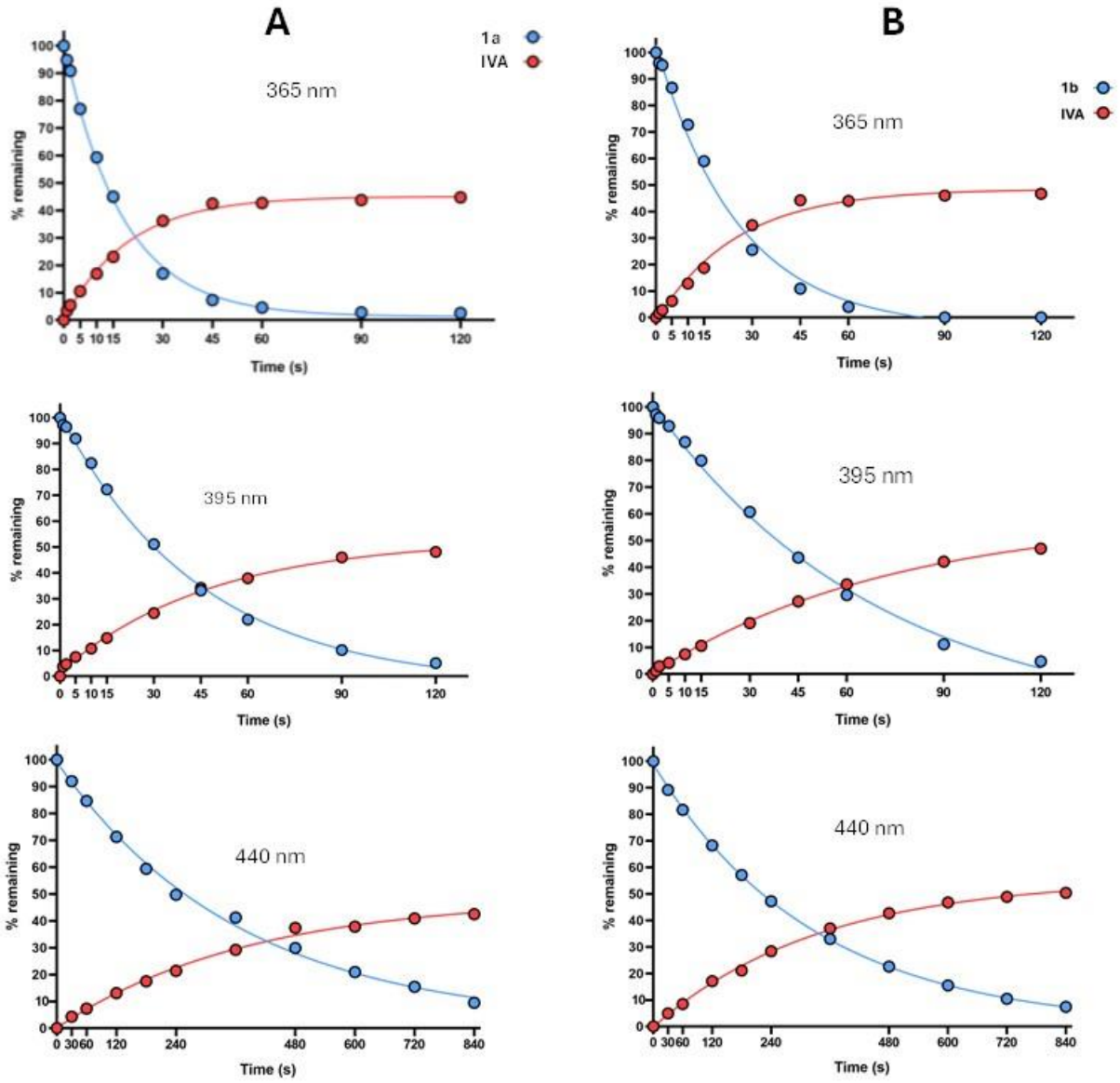

Figure 1. Time courses for the photolysis reaction of **1a** (A) and **1b** (B) (blue circles) upon exposure to 365, 395 and 440 nm light. Also shown is the appearance of the released ivabradine (IVA, red circles). Concentrations were determined by HPLC.

Block of HCN1 channels by photocleavage of BHQ-IVA *in vitro*

To test and characterize the blocking activity of BHQ-IVA (hereafter **1a**) on HCN channel current, we expressed the neuronal subtype RFP-hHCN1 (hereafter HCN1) channels in the mammalian cell line HEK 293T and recorded the current in patch clamp experiments in whole-cell configuration. Figure 2A shows that IVA (green sphere) is an open pore blocker that needs to cross the cell membrane (grey parallel lines) to enter the channel pore cavity (mustard) from the cytosolic side. By taking advantage of the autofluorescence of **1a**, which is excited at 405 nm and visible by its emission at 518 nm, we first verified that this molecule can cross the cell membrane. Figure 2A shows mammalian HEK293T cells incubated for 15 minutes in a buffer without (left) and with (right) 30 μM **1a**: the fluorescent signal (green) accumulated inside the mammalian HEK293T cells and persisted ≥ 10 minutes after removal from the external solution.

After confirming efficient entry of **1a** into cells, its blocking effect on HCN1 current was compared to that of commercial IVA (Sigma, CAS number: 148849-67-6). In the reference experiment reported in Figure 2B, commercial IVA was provided in the extracellular solution at 30 μM, well beyond the saturating concentration that for HCN1 is 15 μM.[9] Since the effect of IVA is usage dependent,[9] we employed a voltage protocol (Figure 2B left) consisting of repetitive (0.2 Hz) activating/deactivating voltage steps from the holding potential of – 20 mV to the test potential of -110 mV and tail potential at +5 mV (see Experimental Section). A representative current trace of HCN1 before (Ctrl) and after reaching the steady state block (IVA) is shown in the center of Figure 2B. A dot plot (Figure 2B right) shows the time course of steady state current amplitude before and during the application of IVA indicated by the horizontal black bar.

In control experiments reported in Figure 2C, we tested possible aspecific effects of the released cage, BHQ-OH, (100 μM) in the dark (data not shown) and in UV light (395 nm, 0.5 mW/mm^2); magenta color indicates exposure to UV light. We further tested **1a** in the dark at 100 μM, to exclude any basal activity (Fig. 2D). In all cases, there was no blocking effect of the compounds. On the contrary, when 30 μM **1a** was either pre-treated for 1 minute with 395 nm UV light (0.5 mW/mm^2) or directly exposed to the same UV-light during perfusion, we recorded a clear block of the HCN1 current (Figure 2E,F). Figures 2E and F show that not only the amount but also the kinetics of block was comparable to that of commercial IVA (compare with Figure 2B). The histogram of Figure 2G summarizes mean fractional blocks: 30 μM **1a** pre-treated with UV exerts the same block (95%) of 30 μM IVA. When 30 μM **1a** was provided in the extracellular solution and illuminated with UV light during perfusion, the block was still very high but for unclear reasons slightly lower (85%). Assuming a release efficiency with UV light (395 nm) around 50% (Table 1), 30 μM **1a** should release 15 μM IVA, still a saturating concentration for HCN1. It is possible that other factors, arising from the combination of the kinetics of release and the kinetics of block contribute to lower the fractional block, even though only marginally.

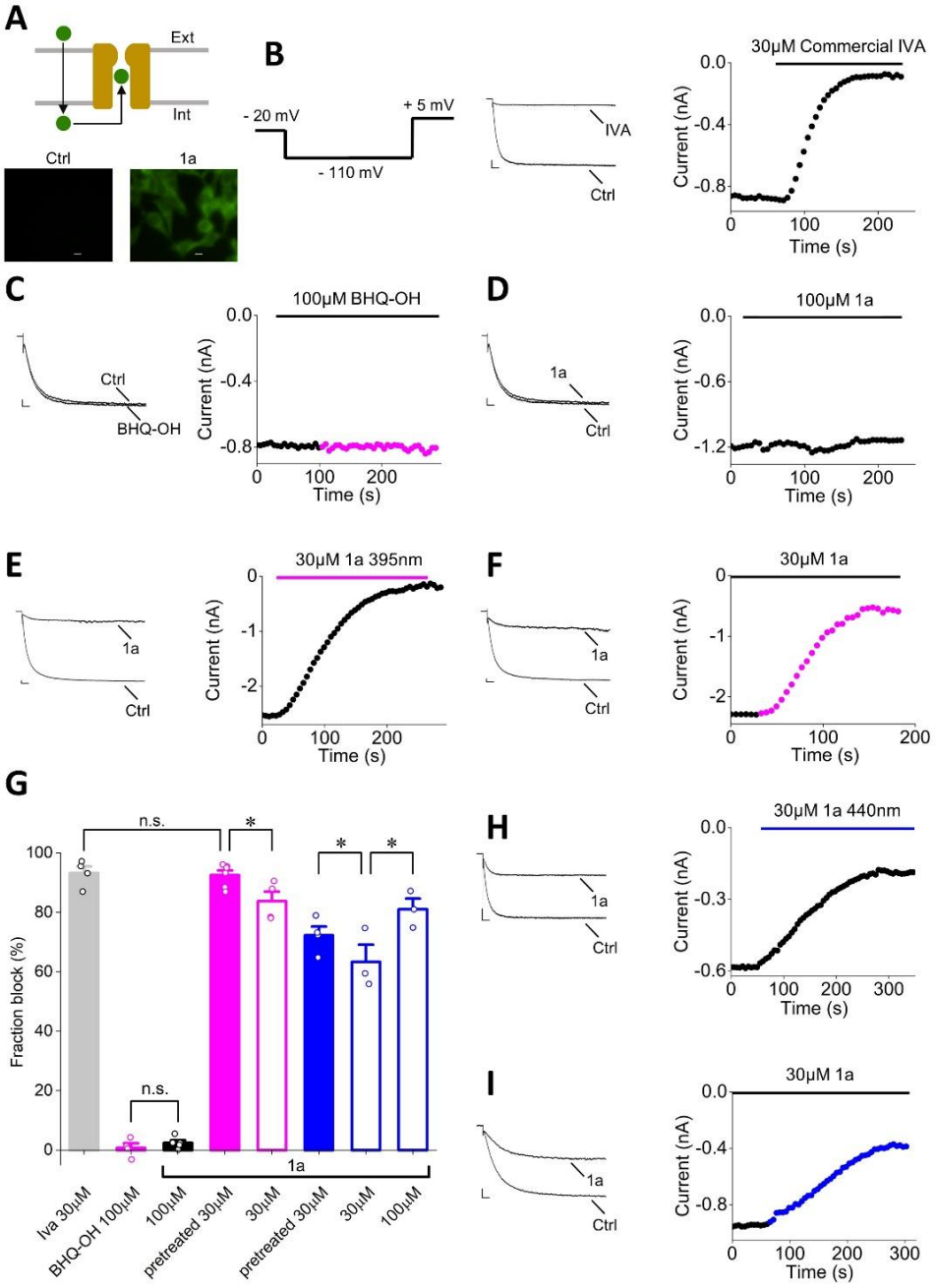

Figure 2: Photocleavage of BHQ-IVA induces block of HCN1 channels expressed in HEK cells. A, (*upper*) Cartoon representation of the mode of action of IVA (green sphere) on HCN channel (mustard) where extracellular (Ext) and intracellular (Int) side of the plasma membrane (parallel gray lines) are indicated; (*lower*) fluorescent microscopy images of HEK293T cells in control solution (Ctr) and after perfusion with 30 µM **1a** for 5 minutes. Images were taken for 10 minutes of washout. Scale bar 5 µm. **B**, Centre: sample current trace before (ctrl) the application and after the full effect of IVA measured with the protocol shown in the left panel. Scale bar is 100 pA x 100 ms. Time-course of current amplitudes recorded at -110 mV before and during the application of 30 µM commercial IVA is shown in right panel (duration indicated by the black bar). **C**, sample current trace recorded at -110 mV before and at the end of the application of 100 µM BHQ-OH (duration indicated by the black bar). Time-course of current amplitudes is shown in the right panel. Steady state currents measured in the presence of a 395 nm light stimulation are shown in magenta. **D**, sample current traces recorded at -110 mV before and at the end of the application of 100 µM **1a** in dark (duration indicated by the black bar). Time-course of current amplitudes is shown in the right panel. **E**, Sample current traces

recorded at -110 mV before and after the full effect of 30 μM **1a**, pretreated at 395 nm (see text). Time course of current amplitude is shown in the right panel. Duration of 30 μM **1a** perfusion is indicated by the magenta bar. **F**, Sample current traces recorded at -110 mV before and after the full effect of 30 μM **1a**. Time course of current amplitude is shown in the right panel. Steady state currents measured in the presence of a 395 nm light stimulation are shown in magenta. Duration of 30 μM **1a** perfusion is indicated by the black bar. **G**, Bar graph shows the fractional current block calculated as the ratio between block-induced current reduction and control current. Full and empty coloured bars indicate that **1a** was provided either in a pretreated form (full bar) or irradiated during the perfusion (empty bar), respectively (see text). Color code as in the other panels (black indicates dark ambient). Mean values ± SEM and number of experiments are IVA 30 μM: 93.2 ± 2.2, n=4; BHQ-OH 100 μM: 0.8 ± 1.5, n=4; **1a** 100 μM: 2.4 ± 0.8, n=5; **1a** 30 μM pretreated at 395 nm: 92.5 ± 1.6, n=6; **1a** 30 μM: 83.7 ± 3.2, n=4; **1a** 30 μM pretreated at 440nm: 72 ± 2.9, n=4; **1a** 30 μM: 63.4 ± 5.8, n=3; **1a** 100 μM: 81 ± 3.5, n=3. * $p<0.05$ by one way Anova followed by post-hoc Fisher test. **H**, Sample current traces recorded at -110 mV before and after the full effect of 30 μM **1a**, pretreated at 440 nm (see text). Time course of current amplitude is shown in the right panel. Duration of 30 μM **1a** perfusion is indicated by the blue bar. **I**, Sample current traces recorded at -110 mV before and after the full effect of 30 μM **1a**. Time course of current amplitude is shown in the right panel. Steady state currents measured in the presence of a 395 nm light stimulation are shown in blue. Duration of 30 μM **1a** perfusion is indicated by the black bar.

As a next step, we tested, in patch clamp experiments, if uncaging of **1a** is also possible with blue light (440 nm), a less harmful wavelength for the cell, in view of medical applications. As shown in Figure 1, this wavelength produces in 1 minute roughly three time less IVA than 395 nm UV light. With a concentration of 30 μM, the blocking effect on HCN1 current was 70% when **1a** was pre-illuminated for 1 minute (440 nm, 1 mW/mm^2) and 65% when **1a** was illuminated during perfusion, confirming the slight difference between the two modalities of uncaging (Figure 2G). This percentage of block (65-75%) corresponds, in HCN1, to that exerted by 3 μM IVA.[9] Increasing the concentration of **1a** to 100 μM enhanced the block to 85% (Figure 2G), showing that the lower uncaging efficiency of blue light can be compensated by a higher concentration of the caged compound. In conclusion, our data show that i) BHQ-OH and **1a** are ineffective on HCN1 in the dark even at high concentrations (**1a** 100 μM), ii) UV light releases from **1a** active IVA that blocks HCN channels with a kinetics and a block efficiency comparable to that of commercial IVA and iii) most important, **1a** can be released by visible (blue) light. The low efficiency of blue light release compared to UV light can be compensated by increasing the initial drug concentration. Before investigating the effect of **1a** ex vivo (brain slices) and in vivo, we tested its cytotoxicity, along with the one of the caging compound BHQ-OH. To this end, we cultured HEK293 T cells in presence of either 100 μM **1a**, 100 μM BHQ-OH or the vehicle (DMSO) and measured their viability at four different incubation times, up to 48h (figure

S2). No significant reduction in cell viability was observed over the 48h of treatment with respect to the controls, indicating no apparent cytotoxic effect of the compounds, at least in HEK293 T cells.

Photocleavage of BHQ-IVA efficiently reduces native I_h current in brain slices

To test the effect of BHQ-IVA on the neuronal, HCN-driven, current I_h, we performed patch clamp experiments in neurons on mouse brain slices. Dendritic recordings were performed on L5 neurons in the medial pre-frontal cortex (age of the animal ~16 weeks; average distance from soma 185 ± 30 μm) (Figure 3A). I_h was evoked in voltage clamp configuration by applying a hyperpolarizing step from -70 to -120 mV. Subsequent perfusion of 100 μM BHQ-OH in presence of a 365 nm UV light stimulation (magenta) did not alter the I_h current properties. Bath perfusion of 30 μM Ivabradine in contrast significantly reduced I_h current (Figure 3B). Average pooled data for control, BHQ-OH and 30 μM commercial IVA are shown in right panel.

Figure 3C shows exemplary current trace recorded before (control) and after activation of 30 μM or 100 μM **1a** (top and bottom left panels respectively) with light at 365 nm; light was delivered by directly illuminating the brain slice during the patch clamp recording. The center column shows average pooled data for the current reduction; the right column shows the time course of the normalized steady state current amplitude just before (first dot) and during the application of either 30 μM or 100 μM IVA (top and bottom, respectively). Black bars indicate duration of **1a** superfusion at the indicated concentration. Colored symbols denote the stimulation with 365 nm light.

In these neurons, I_h is responsible for a prominent depolarizing voltage "sag" in response to a steady hyperpolarizing current recorded under current clamp. Figure 3D shows the typical voltage “sag” in response to a –140 pA hyperpolarizing current injection before (control) and after activation of 30 μM or 100 μM **1a** by constant illumination with 365 nm light. The “sag” amplitude was calculated as

the maximum membrane hyperpolarization following current onset minus the steady state potential prior to onset of the hyperpolarizing current injection. Average pooled data before drug application (Ctrl) and after reaching the full light induced drug effect (365 nm) are shown in right panels (same pool of cells shown in panel C). The light triggered inhibition of the I_h current is reflected in the reduction of the "sag" amplitude. Exposure of cells in the same kind of experiments to blue light (G) confirms that this light wavelength (470 nm) is equally effective than UV light in reducing I_h current in neurons in terms of amount (center) and kinetics (right panel).

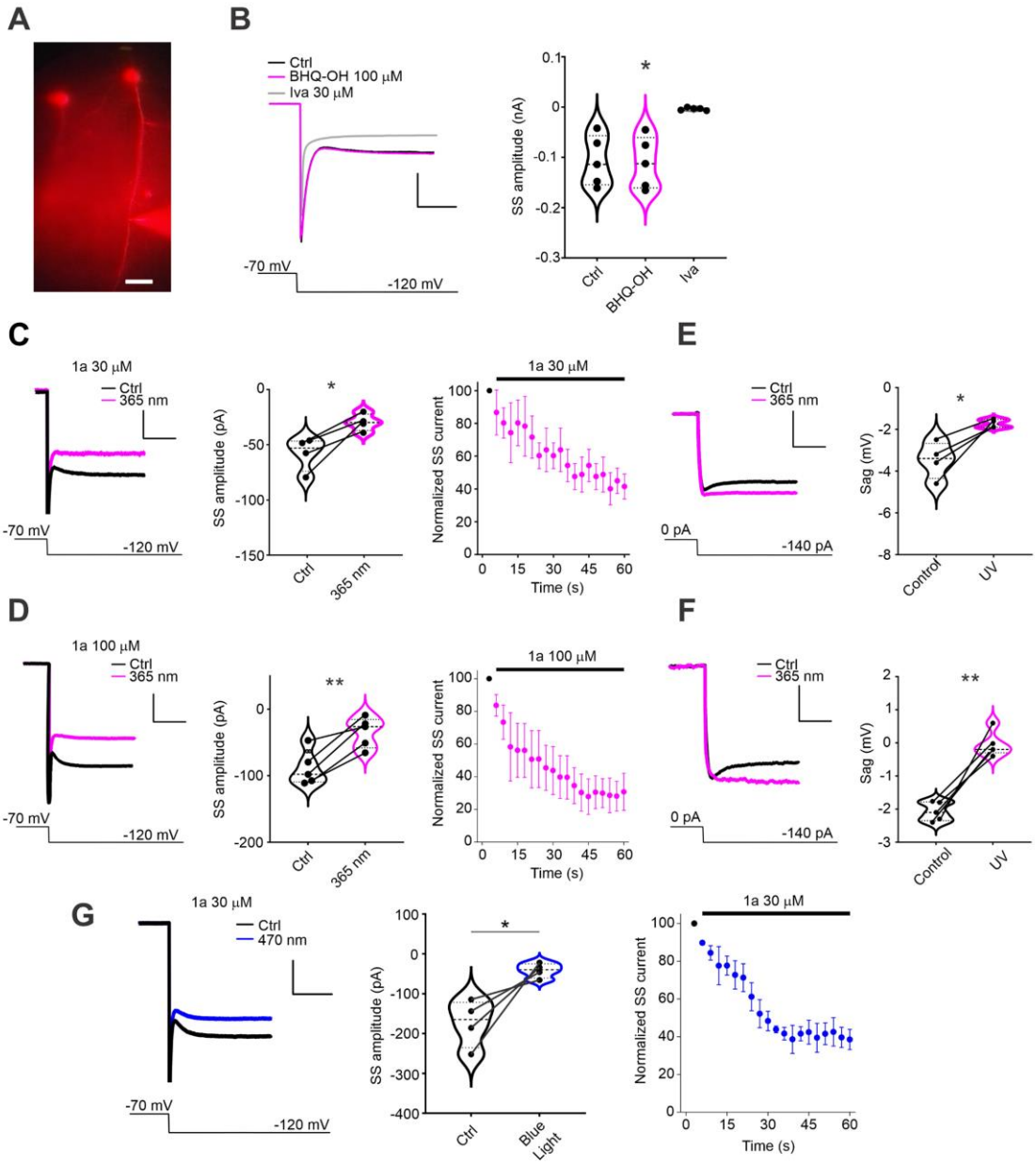

Figure 3: Photocleavage of BHQ-IVA blocks native I_h current in neurons.

A, 6 dendritic recordings were performed on L5 neurons in the medial prefrontal cortex (age of the animal ~16 weeks; average distance from soma 185 ± 30 mm). **B**, *left panel*: I_h was evoked in voltage clamp configuration by applying an hyperpolarizing step from -70 to -120 mV. Subsequent perfusion of 100 μM BHQ-OH in presence of a 365 nm light stimulation (magenta) did not alter the I_h current properties while bath perfusion of 30 μM IVA significantly reduced I_h current. Scale bar is 100 pA x 15 ms. *right panel*: Average pool data for control, BHQ-OH and 30 μM commercial IVA are shown. **C,** left panel shows exemplary current trace recorded before (control) and after activation of 30 μM **1a** with 365 nm light stimulus (365 nm, 23.5 mW) delivered by directly illuminating the brain slice during the patch clamp recording. Scale bar is 100 pA x 15 ms. Analyses of the steady state current before drug application (ctrl) and after reaching the full effect (365 nm) are shown in center panel. Right panel shows time course of the normalized steady state current amplitude just before (first dot, black) and during the application of 30 μM **1a**. Black bars indicate **1a** superfusion. Colored symbols denote the stimulation at 365 nm light. Values show mean ± SEM. **D,** left panel shows exemplary current trace recorded before (control) and after activation of 100 μM **1a** with 365 nm light stimulus (365 nm). Analyses of the steady state current before drug application (ctrl) and after reaching the full effect (365 nm) are shown in center panel. *p<0.05 **p<0.01 with paired t-student test. Right panel shows time course of the normalized steady state current amplitude just before (first dot) and during the application of 100 μM **1a**. Values show mean ± SEM. **E**, Typical voltage "sag" in response to a –140 pA hyperpolarizing current injection before (control) and after activation of 30 μM **1a** with a 365 nm light (365nm). Scale bar is 10 mV x 200 ms. "sag" amplitude was calculated as the maximum membrane hyperpolarization following current onset minus the steady state potential prior to offset of the hyperpolarizing current injection. Average pool data before the drug application (ctrl) and after reaching the full effect (365 nm) are shown in the right panel (same pool of cells shown in panel C). **F**, Typical voltage "sag" in response to a –140 pA hyperpolarizing current injection before (control) and after activation of 100 μM **1a** with a 365 nm light (365 nm). Scale bar is 10 mV x 200 ms. Average pool data before the drug application (ctrl) and after reaching the full effect (365 nm) are shown in the right panel (same pool of cells shown in panel D). **G**, left panel shows exemplary current trace recorded before (control) and after activation of 30 μM **1a** with 470 nm light stimulus (470nm). Analyses of the steady state current and tail currents before drug application (control) and after reaching the full effect (blue light) are shown in the left and centre panel, respectively. Right panel shows time course of the normalized steady state current amplitude just before (first dot) and during the application of 30 μM **1a**.

Photocleavage of BHQ-IVA reduces the heart rate of zebrafish

We next investigated whether **1a** and **1b** can block HCN channels *in vivo* in zebrafish.

Zebrafish HCN4 orthologs are expressed in the heart and contribute to heart rate regulation, as known in the human heart.[30] Zebrafish are transparent in the early stages of development, and this provides two advantages to our study: first, the heart is visible from the outside of the body and the heart rate can be directly monitored; second, **1a** or **1b** can be easily uncaged by light.

We injected 1-2 nL of 1 mM **1a** or **1b** into the pericardial region of zebrafish larvae at 48 hpf; as a control, the same volume of vehicle (0.1% DMSO) was injected. After injection, zebrafish hearts were light-stimulated at 365 nm (0.5 mW/mm^2) for 2 min or at 436 nm (2 mW/mm^2) for 10 min. Illumination at 365 nm reduced the heart rates of control zebrafish to 84±1% after 2 minutes.

However, the heart rate reduction of zebrafish injected with **1a** or **1b** were much more prominent reaching 51±2% and 49±1%, respectively, of the starting value (Figure 4 A-C). Illumination at 436 nm for 10 min reduced the heart rates of control zebrafish to 80±1%. The heart rates of zebrafish injected with **1a** or **1b** were in contrast reduced to 49±4% and 51±2%, respectively (Figure 4 D-F). As expected, it took longer to photoactivate **1a** and **1b** at 436 nm (Figure 4F). At the same time, data in Figure 4F show that, in blue light, the kinetics of inhibition is faster with **1b** than with **1a**. This reflects the finding that illumination with blue light in vitro uncages **1b** at a faster rate (see Table 1 and Figure 1).

In summary, **1a** and **1b** after uncaging effectively reduced the heart rate in zebrafish by blocking HCN channels to the same extent previously reported for IVA.[30]

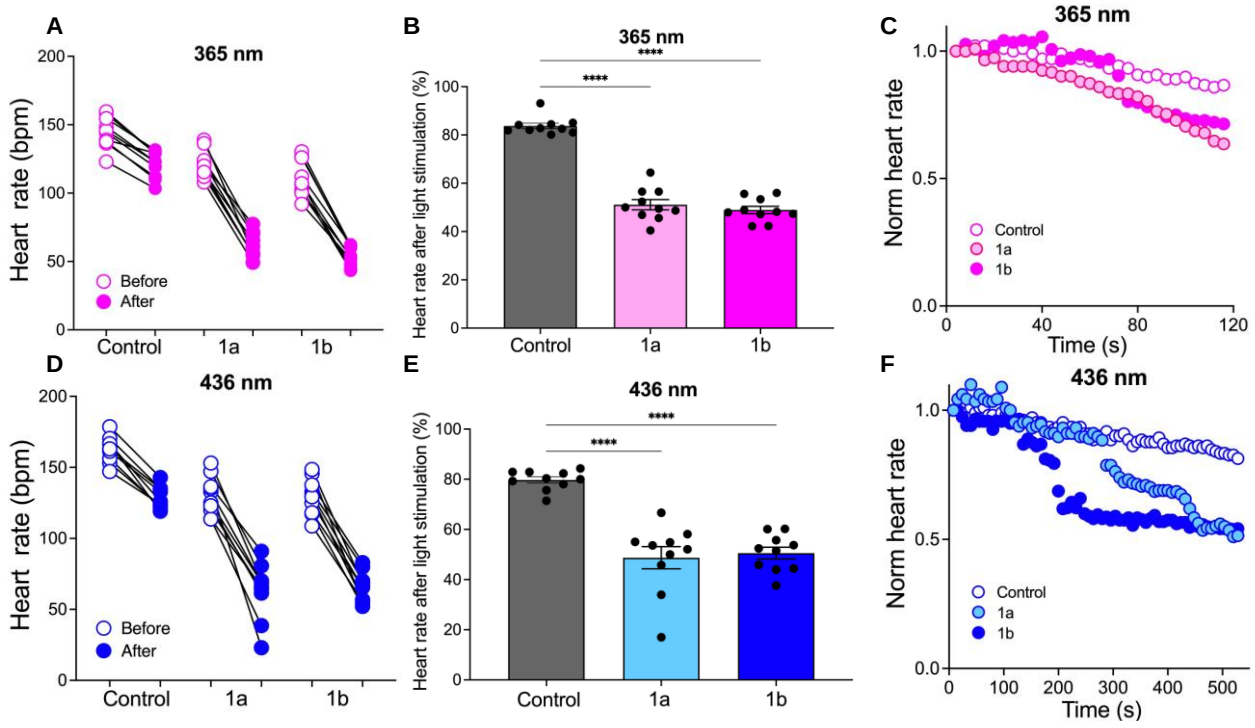

Figure 4: Photocleavage of BHQ-IVA reduces zebrafish heart rate.

A, heart rate changes before and after two minutes of illumination with 365 nm light (n = 10). Zebrafish larvae at 48 dpf were injected with approx 1-2 nL of either control vehicle (0.1% DMSO), **1a** (1 mM), or **1b** (1 mM). **B**, heart rate reduction after two minutes of illumination with 365 nm light (n = 10 for each). Error bars: mean ± SEM. Statistical analysis was performed using Dunnett's test. **** indicates $p<0.0001$. **C**, time course of normalized heart-rate change in zebrafish injected with control (white), **1a** (pink), or **1b** (magenta) during 365 nm illumination. **D**, heart rate changes before and after ten minutes of illumination with 436 nm light (n = 10). Zebrafish larvae at 48 dpf were injected with either control vehicle (0.1% DMSO), **1a** (1 mM), or **1b** (1 mM). **E**, heart rate reduction after ten minutes of illumination with 436 nm light (n = 10 for each). Error bars: mean

± SEM. Statistical analysis was performed using Dunnett's test. **** indicates p<0.0001. **F**, time course of normalized heart-rate change in zebrafish injected with control (white), **1a** (light blue), or **1b** (blue) during 436 nm illumination.

In vitro plasma stability study

After validating the effects of BHQ-IVA *in vitro*, *ex vivo* and *in vivo* upon uncaging irradiation, we investigated its *in vitro* stability in the presence of human plasma within 24 hours. The results revealed that BHQ-IVA remained stable in human plasma for up to 24 hours (Fig. 5).

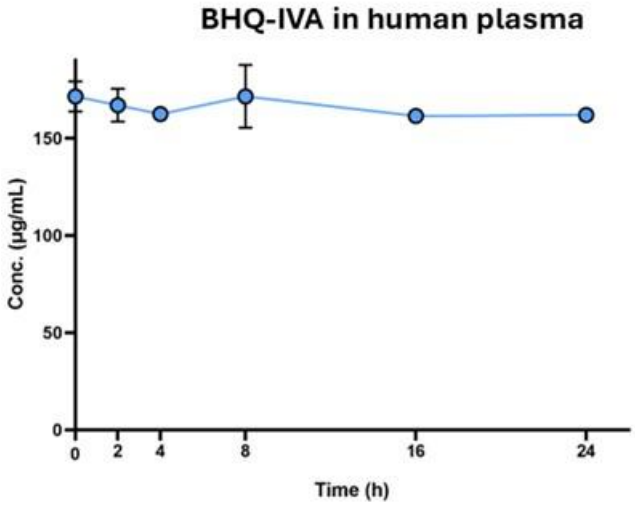

Figure 5. Stability study *in vitro* of BHQ-IVA (1b) in human plasma within 24 h.

Conclusions

There are several acute and chronic diseases related to HCN channels dysfunction in distinct body organs that would benefit from the controlled release, in space and time, of their subtype-aspecific antagonist IVA. Our strategy to endow IVA with photoremovable cage, 8-bromo-7-hydroxy-2-quinolinylmethyl (BHQ), was successful and the newly synthesized caged IVA molecule, BHQ-IVA, was efficiently released by UV and, most important, by visible blue light in biological validation conducted *in vitro*, *ex vivo* and *in vivo*. Data confirm that BHQ-IVA is membrane permeant and accumulates inside the cells, as needed for this open channel blocker. Furthermore, BHQ-IVA and its

photoreleased cage BHQ-OH show no apparent toxicity for cells. In vitro experiments have shown that the block of HCN current achieved with UV light was comparable to that of commercial IVA in terms of kinetics and intensity of block. Even though the rate of the release by blue light was less efficient than by UV light, this deficit could be compensated for by adjusting the BHQ-IVA concentration. Ex vivo experiments, performed in brain slices, and in vivo experiments with zebrafish confirmed efficient inhibition of the native I_f/I_h current leading to the desired pharmacological effect of reduction of the "sag" amplitude in the voltage response of neurons and of slowing of the heart rate in zebrafish. Besides its immediate use as a research tool, we see a great potential in this approach for developing protocols in which the HCN blocker is activated on demand in a patient in an organ of interest. Our strategy allows to restrict exposure to IVA at the organ of interest only, reducing unwanted side effects on other HCN subtypes in other organs. This aspect is crucial for the treatment of HCN related diseases that affect the nervous system as systemic administration of IVA unavoidably leads to reduced heart rate. BHQ-IVA is therefore a promising prototype for developing novel therapeutic approaches.

Experimental section

Chemistry

All chemicals and solvents were used as received from commercial sources or prepared as described in the literature. Flash chromatography purifications were performed using Biotage® IsoleraTM equipped with KP-Sil 32–63 μm 60 Å cartridges. TLC analyses were carried out on alumina sheets precoated with silica gel 60 μm having a fluorescent indicator (Macherey-Nagel Alugram® SilG/UV 254). The spots were seen under UV light (λ = 254nm); Rf values are given for guidance. ^{1}H and ^{13}C NMR spectra were recorded with a Varian Mercury 300 spectrometer and elaborated with MNova ® software. Chemical shifts are expressed in ppm to residual solvent (MeOH or DMSO) as internal standard. Melting points were obtained using Buchi Melting Point B-540 apparatus. UV-Vis analyses

were recorded using a Shimadzu® UV-1900 UV-Vis spectrophotometer in the 600nm-200nm range. Emission spectra were acquired with a Jasco FP-750 spectrofluorometer. Each compound was dissolved in a 1:1 DMSO:water mixture to a 10 mM concentration to obtain stock solutions. All chromatographic runs were performed on Hewlett Packard series 1050 UV-Vis HPLC using a Vision HT C18 Classic column (particle size 5µm, 250 x 4.6 mm dimensions), monitoring the AUC at 280 nm wavelength. Separations were obtained with a solvent gradient elution (flux rate 1.5 mL/min) using a mobile phase consisting in A= 0.1% TFA in water and B= 0.1% TFA in acetonitrile; the gradient started with a 30% B to 50% in 9 min, followed by a return to 30% B in 3 min and a re-equilibration for 2 min before the next run. **1a**, **1b**, and commercially available ivabradine were >95% pure by HPLC analysis (see chromatograms in Supporting Information).

*8-Bromo-7-methoxymethoxy-2-methylquinoline (**3**)*

8-Bromo-7-hydroxy-2-methylquinolin-1-ium-4-metylbenzenesulfonate (**2**) (2.79 g, 6.80 mmol) was suspended in anhydrous DCM (12 mL). DIPEA (2.4 mL, 13.60 mmol) was added. The resulting mixture was stirred for 30 min at rt. MOMBr (0.83 mL, 10.20 mmol) was added dropwise at 0 °C and then the solution was left stirring at rt overnight. NaOH 1M (10 mL) was added to the solution and the two phases were separated. The organic phase was dried over anhydrous sodium sulphate and the solvent was evaporated under reduced pressure to give a crude, which was purified by flash chromatography using petroleum ether:EtOAc from 9:1 to 6:4 as eluent. 8-Bromo-7-methoxymethoxy-2-methylquinoline (**3**) (1.18 g, 4.17 mmol 61%) was obtained as a yellow oil. **Rf** (petroleum ether/EtOAc 7:3) 0.30, **^{1}H NMR** (300 MHz, CDCl3) δ 7.98 (d, *J* = 8.3 Hz, 1H), 7.69 (d, *J* = 8.9 Hz, 1H), 7.43 (d, *J* = 8.9 Hz, 1H), 7.25 (d, *J* = 5.4 Hz, 1H), 5.39 (s, 2H), 3.57 (s, 3H), 2.80 (s, 3H).

*8-Bromo-7-methoxymethoxyquinoline-2-carbaldehyde (**4**)*

8-Bromo-7-methoxymethoxy-2-methylquinoline (**3**) (1.18 g, 4.17 mmol) was dissolved in 1,4-dioxane (10 mL). Selenium oxide (0.56 g, 5.01 mmol) was added to the solution and the resulting suspension was left stirring at 80 °C for 1h. After cooling, the suspension was filtered and the filtrate was concentrated at reduced pressure to give 8-bromo-7-methoxymethoxyquinoline-2-carbaldehyde (**4**) (1.24 g, 4.17 mmol, 100%) as a white solid. **Mp** 129.9-130.8 °C, **Rf** (Cyclohexane/EtOAc 8:2) 0.27, **^{1}H NMR** (300 MHz, CDCl3) δ 10.29 (s, 1H), 8.27 (d, J = 8.4 Hz, 1H), 7.97 (d, J = 8.3 Hz, 1H), 7.83 (d, J = 9.1 Hz, 1H), 7.65 (d, J = 9.0 Hz, 1H), 5.44 (s, 2H), 3.59 (s, 3H).

*(8-Bromo-7-methoxymethoxyquinoline-2-yl)methanol (**5**)*

8-Bromo-7-methoxymethoxyquinoline-2-carbaldehyde (**4**) (1.28 g, 4.31 mmol) was dissolved in ethanol and sodium boron hydride was added in portions. The reaction mixture was left stirring at rt for 1h. Water was added and ethanol was evaporated at reduced pressure. The resulting crude product was extracted with EtOAc (3x20 ml). The combined organic phases were dried with anhydrous sodium sulfate and the solvent evaporated under reduced pressure to give (8-bromo-7-methoxymethoxyquinolin-2-yl)methanol (**5**) (1.09 g, 3.66 mmol, 85%) as a yellow oil. **Rf** (Cyclohexane/EtOAc 8:2) 0.10, **^{1}H NMR** (300 MHz, $CDCl_3$) δ 8.08 (d, J = 8.4 Hz, 1H), 7.76 (d, J = 9.0 Hz, 1H), 7.50 (d, J = 9.0 Hz, 1H), 7.22 (d, J = 8.4 Hz, 1H), 5.42 (s, 2H), 4.94 (s, 2H), 4.79 (bs, 1H), 3.59 (s, 3H).

*(8-Bromo-7-methoxymethoxyquinoline-2-yl)methyl methanesulfonate (**6**)*

(8-Bromo-7-methoxymethoxyquinolin-2-yl)methanol (**5**) (1.09 g, 3.66 mmol) was dissolved in DCM; TEA (1.5 mL, 10.98 mmol) was added. To the stirred solution at 0 °C, methanesulfonyl chloride (0.60 mL, 7.69 mmol) was added dropwise. The solution was left stirring at 0 °C for 1h. Water was added and the two layers were separated. The organic phase was washed with brine, dried with anhydrous sodium sulfate and the solvent evaporated under reduced pressure to give the crude

product that was purified by flash chromatography using cyclohexane:EtOAc from 9:1 to 7:3 as eluent. (8-Bromo-7-methoxymethoxyquinolin-2-yl)methyl methanesulfonate (**6**) (0.92 g, 2.45 mmol, 67%) was obtained as a light pink solid. **mp** 110.3-112.1 °C, **Rf** (Cyclohexane/EtOAc 8:2) 0.13, **^{1}H NMR** (300 MHz, $CDCl_3$) δ 8.19 (d, J = 8.4 Hz, 1H), 7.79 (d, J = 9.0 Hz, 1H), 7.59 – 7.48 (m, 2H), 5.57 (s, 2H), 5.42 (s, 2H), 3.58 (s, 3H), 3.23 (s, 3H).

(8-Bromo-7-hydroxyquinoline-2-yl)methyl methanesulfonate (7)

Trifluoroacetic acid (2.6 mL, 34.50 mmol) was added to a solution of (8-bromo-7-methoxymethoxyquinolin-2-yl)methyl methanesulfonate (**6**) (1.45 g, 3.45 mmol) in DCM (15 mL). The resulting solution was stirred at rt for 8 h and then washed with H_2O (5 mL). The layers were separated. The aqueous layer was extracted with EtOAc (2 x 7 mL). The combined organic phases were dried (Na_2SO_4) and concentrated under reduced pressure to give the crude product. Purification by flash chromatography with 10:0 to 7:3 cyclohexane-acetone as eluent gave (8-bromo-7-hydroxyquinolin-2-yl)methyl methanesulfonate (**7**) (1.03 g, 3.10 mmol, 90%) as a light grey solid, **mp** 132-134 °C; **Rf** (Cyclohexane/Acetone 7:3) 0.17; **^{1}H NMR** (300 MHz, CDCl3): δ 8.18 (d, J = 8.4 Hz, 1H), 7.74 (d, J = 8.8 Hz, 1H), 7.50 (d, J = 8.4 Hz, 1H), 7.37 (d, J = 8.8 Hz, 1H), 5.55 (s, 2H), 3.20 (s, 3H).

*(S)-N-(8-bromo-7-hydroxyquinolin2-yl)methyl-3-(7,8-dimethoxy-2-oxo-1,2,4,5-tetrahydro-3H-benzo[d]azepin-3-yl)-N-(3,4-dimethoxybicyclo[4.2.0]octa-1,3,5-trien-7-yl)methyl-N-methylpropan-1-aminium methanesulfonate (**1a**) (BHQ-IVA mesylate)*

Ivabradine hydrochloride (270 mg, 0.53 mmol) and 1M NaOH (5 mL) were stirred for 10 min at room temperature. The mixture was extracted with EtOAc (3 x 10mL); the collected organic phases were dried over anhydrous sodium sulfate and the solvent was evaporated. Ivabradine (250 mg, 0.53 mmol)

was dissolved in acetonitrile (5 mL) and (8-bromo-7-hydroxyquinolin-2-yl)methyl methanesulfonate (230 mg, 0.69 mmol) was added. The solution was stirred at reflux for 3h. The solvent was evaporated under reduced pressure and the residue was purified by flash chromatography using a gradient of an eluent mixture consisting in DCM:MeOH from 95:5 to 80:20. The product (BHQ-IVA_mesylate) was obtained as a light orange powder (167 mg, 0.21 mmol, 39%); **mp** 139.1-140.6 °C; **R_f** (DCM:MeOH 90:10) 0.21;

^{1}H NMR (300 MHz, CD_3OD) δ 8.36 (d, J = 8.3 Hz, 1H), 7.85 (d, J = 9.1 Hz, 1H), 7.50 (d, J = 8.3 Hz, 1H), 7.36 (d, J = 9.1 Hz, 1H), 6.83 – 6.79 (m, 1H), 6.77 (s, 1H), 6.60 (s, 2H), 4.96 – 4.87 (m, 2H), 4.36 – 4.27 (m, 0.5H), 4.24 – 4.14 (m, 0.5H), 4.13 – 4.02 (m, 1H), 4.00 – 3.86 (m, 1H), 3.81 – 3.66 (m, 19H), 3.61 – 3.55 (m, 2H), 3.41 – 3.38 (m, 3H), 3.11 – 2.97 (m, 3H), 2.72 (s, 3H), 2.36 – 2.20 (m, 2H).

^{1}H NMR (300 MHz, DMSO-d_6) δ 11.18 (bs, exchange with D_2O 1H), 8.47 (d, J = 8.3 Hz, 1H), 7.94 (d, J = 8.9 Hz, 1H), 7.58 (d, J = 8.3 Hz, 1H), 7.44 (d, J = 9.1 Hz, 1H), 6.81 (s, 2H), 6.69 (s, 1H), 6.64 (s, 1H), 4.99 – 4.87 (m, 2H), 4.19 – 3.91 (m, 3H), 3.76 – 3.63 (m, 19H), 3.44 – 3.36 (m, 2H), 3.35 – 3.27 (m, 3H), 3.09 – 2.90 (m, 3H), 2.31 (s, 3H), 2.26 – 2.09 (m, 2H).

^{13}C NMR (100 MHz, CD_3OD) δ 174.21, 156.90, 151.19, 150.76, 150.71, 150.05, 148.22, 147.36, 146.15, 138.18, 134.82, 134.32, 128.06, 127.72, 123.48, 123.09, 120.28, 119.98, 113.98, 113.57, 107.61, 107.32, 106.31, 63.73, 60.24, 59.95, 55.63, 55.60, 55.46, 55.08, 43.71, 41.26, 38.12, 36.02, 35.96, 35.88, 31.38, 21.72.

HRMS (ESI+): calc. for $C_{37}H_{42}N_3O_6Br$: theor. 704.2335; found $[M]^+$: 704.2335

*(S)-N-(8-bromo-7-hydroxyquinolin2-yl)methyl-3-(7,8-dimethoxy-2-oxo-1,2,4,5-tetrahydro-3H-benzo[d]azepin-3-yl)-N-(3,4-dimethoxybicyclo[4.2.0]octa-1,3,5-trien-7-yl)methyl-N-methylpropan-1-aminium hydroxide (**1b**) (BHQ-IVA hydroxide)*

Another batch of crude product, resulting from the same reaction on 250 mg of starting ivabradine, was purified by flash chromatography using a different eluent mixture consisting in 9:1+1% DCM:MeOH+NH_3. BHQ_IVA was isolated as a hydroxide, instead of mesylate salt, as an orange solid (273 mg, 0.38 mmol, 71%); **mp** 154.6-155.9 °C; **R_f** (DCM:MeOH 90:10) 0.21.

^{1}H NMR (400 MHz, CD_3OD) δ 8.05 (d, J = 8.1 Hz, 1H), 7.54 (d, J = 8.9 Hz, 1H), 7.17 (d, J = 8.9 Hz, 1H), 7.10 (d, J = 8.1 Hz, 1H), 6.82 – 6.76 (m, 1H), 6.74 (s, 1H), 6.61 – 6.54 (m, 2H), 4.80 – 4.64 (m, 2H), 4.38 – 4.25 (m, 0.5H), 4.22 – 4.11 (m, 0.5H), 4.06 – 3.96 (m, 1H), 3.96 – 3.81 (m, 1H), 3.80 – 3.67 (m, 13H), 3.64 – 3.31 (m, 11H), 3.08 – 2.97 (m, 1H), 2.97 – 2.88 (m, 2H), 2.33 – 2.04 (m, 2H).

^{13}C NMR (100 MHz, CD_3OD) δ 175.48, 167.88, 152.50, 151.38, 150.27, 150.22, 149.55, 148.90, 148.70, 138.41, 136.16, 135.74, 129.08, 128.27, 127.27, 124.55, 122.55, 117.80, 115.34, 114.95, 108.96, 108.64, 108.44, 68.37, 65.40, 65.18, 61.24, 60.85, 57.01, 56.83, 56.46, 45.03, 42.60, 37.45, 37.40, 32.59, 22.96.

HRMS (ESI+): calc. for $C_{37}H_{42}N_3O_6Br$: theor. 704.2335; found $[M]^+$: 704.2336

Biology

Electrophysiology and in-vitro cytotoxicity in HEK 293 T cells

Patch clamp recordings were carried out on HEK293T cells cultured in DMEM high glucose medium (Euroclone) supplemented with 10% FBS (Euroclone) and 1% Penicillin-Streptomycin (Sigma). Cells were grown at 37 °C with 5% CO_2. When 70% confluent, cells were transfected (in a 35 mm petri dish) with Turbofect transfection reagent (Thermo Fisher) using 1 µg of human HCN1 cDNA previously cloned in frame at the C-terminus of RFP contained in a mammalian expression vector.

After 24h from the transfection, cells were trypsinized and dispersed in 35 mm petri dishes. Red fluorescent isolated cells were selected for patch clamp by means of an inverted fluorescent

microscope. HCN1 currents were recorded at room temperature, in whole cell configuration, using an ePatch (Elements srl) or a Axopatch 200b amplifier (Molecular Devices). Signals acquired with the Axopatch 200b were digitized using a Digidata 1550B (Moelcular Devices). Patch-clamp signals were acquired with a sampling rate of 5 kHz and lowpass filter at 1 kHz. Patch pipettes were pulled using a P-97 micropipette puller (Sutter, Novato, CA) and had resistances ranging from 4 to 6 MΩ. Patch pipettes were filled with a solution containing 10 mM NaCl, 130 mM KCl, 1 mM egtazic acid (EGTA), 0.5 mM $MgCl_2$, 2 mM ATP (magnesium salt), and 5 mM HEPES–KOH buffer (pH 7.4). The extracellular bath solution contained 110 mM NaCl, 30 mM KCl, 1.8 mM $CaCl_2$, 0.5 mM $MgCl_2$, and 5 mM HEPES–KOH buffer (pH 7.4). The voltage step protocol used for block investigation consisted of activating/deactivating steps (−110 mV, 1.8 s; +5 mV, 0.5 s) applied every 5.5 s from a holding potential of −20 mV.

Commercial Ivabradine (Sigma, CAS number: 148849-67-6) was dissolved in MilliQ water at 10 mM (stock concentration) and added to the extracellular solution at the indicated concentration by the means of a pinch valve perfusion system. **1a** was dissolved in 50% DMSO and 50% MilliQ water (DMSO was added first) at 10mM (stock concentration) and added to the extracellular solution as described for the commercial version. The molecule was provided either in a light pretreated form or uncaged during the perfusion (see text). The pretreatment was performed by exposing the stock solution contained in a small tube to the light coming out from the optical fiber of the SPECTRA-X device (Lumencor) either at 395 nm (0.5 mW/mm^2) or at 440 nm (1 mW/cm^2). Subsequenlty, the so-treated stock solution was added to the extracellular bath solution and loaded in the perfusion system. The uncaging during the perfusion was performed by placing the optical fiber near the cell impaled by the patch clamp electrode. Light intensities are the same used for pre-treatment. The spectral output at 365 nm or 440 nm declared by the manufacturer is shown in 6A.

Cytotoxicity studies were performed in HEK293T cells cultured in 35 mm petri dishes using DMEM high-glucose supplemented with 10% FBS and 1% PenStrep. When a 80-90% confluency was

reached, 100 µM **1a** or 100 µM BHQ-OH were added to the growth medium. Control samples consisted of untreated cells and cells treated with 0.5% DMSO. After four different incubation times (8h, 16h, 24h, 48h) cells were detached from the petri dishes, centrifuged, and resuspended in a PBS solution containing a viability fluorescent dye (LIVE-DEAD NearIF by Thermo Fisher). A positive control was included within each time point by heating a sample of untreated cells at 60 °C for 20 minutes. Cells were visualized by fluorescence microscopy with a 20X objective using an excitation wavelength of 640 nm and counted. Three random quadrants were selected from each triplicate for quantification of dead cells.

Electrophysiology on brain slices

Acute slice preparation began with the anesthesia of mice using a ketamine/xylazine combination (100 mg/kg, 10 mg/kg), followed by perfusion through the heart with ice-cold saline solution composed of the following (in mM): 2.5 KCl, 1.25 NaH_2PO_4, 25 $NaHCO_3$, 0.5 $CaCl_2$, 7 $MgCl_2$, 7 dextrose, 205 sucrose, 1.3 ascorbate, and 3 sodium pyruvate (bubbled with 95% O2/5% CO2 to maintain pH at approximately 7.4). Sections, 250 µm thick (300 µm for mPFC), were obtained using a vibrating tissue slicer (Leica VT S1000, Germany). These slices were then incubated for 30 minutes at 35 °C in a chamber filled with aCSF containing the following (in mM): 125 NaCl, 2.5 KCl, 1.25 NaH_2PO_4, 25 $NaHCO_3$, 2 $CaCl_2$, 2 $MgCl_2$, 10 dextrose, and 3 sodium pyruvate (bubbled with 95% O_2/5% CO_2) before being maintained at room temperature until recording. Five male mice aged 2 to 3 months were used for this part of the experiment.

For patch clamp experiments, slices were placed in a submerged, heated (32 °C–34 °C) recording chamber, continuously perfused (1-2 ml/minute) with bubbled aCSF containing the following (in mM): 125 NaCl, 3.0 KCl, 1.25 NaH_2PO_4, 25 $NaHCO_3$, 2 $CaCl_2$, 1 $MgCl_2$, 10 dextrose, 3 sodium pyruvate, 0.025 D-APV, 0.02 DNQX, 0.005 CGP, and 0.002 gabazine. Slices were observed either with an Axioskop microscope (Carl Zeiss) and differential interference optics or an AxioExaminer D

microscope (Carl Zeiss) and Dodt contrast optics. Patch pipettes (4–8 MV) were pulled from borosilicate glass and coated with Parafilm to minimize capacitance. The pipette solution contained the following (in mM): 120 K-gluconate, 16 KCl, 10 HEPES, 8 NaCl, 7 K2 phosphocreatine, 0.3 Na-GTP, 4 Mg-ATP, pH 7.3 with KOH. In some experiments, specific substances were added to the internal recording solution. Alexa-594 (16 mM; Thermo Fisher Scientific, #A10428) was included in the internal recording solution to ascertain the dendritic recording location relative to the soma. Data were collected using a Multiclamp 700b amplifier and Clampex11 (Molecular Devices) data acquisition software, at 10–50 kHz, filtered at 2–10 kHz, and digitized by an Axon Digidata 1550B interface (Molecular Devices). Pipette capacitance was adjusted, and the bridge was balanced during each recording. Series resistance was monitored and adjusted throughout each experiment, being 10-25 MOhm for somatic recordings and 15–40 MOhm for dendritic recordings. Recordings were discarded if series resistance increased by more than 30% during the recording. Voltages were not adjusted for the liquid-junction potential (estimated as approximately -8 mV).

I_h was elicited in voltage clamp configuration by applying a series of activating/deactivating steps (-120 mV, 1.8 sec; + 5 mV, 0.15 sec) from a holding potential of −70 mV. Voltage "sag" was measured by injecting a negative current pulse (-140 pA, 1 sec) before the application of **1a** and after reaching the full effect. "Sag" amplitude was calculated as the maximum membrane hyperpolarization following current onset minus the steady state potential prior to offset of the hyperpolarizing current injection.

Both commercial Ivabradine and **1a** stock solutions were prepared as described above (see "electrophysiology on HEK 293 T cells"), diluted in the aCSF solution at the concentration specified in the text and perfused to the sample.

For light stimulation, light pulses were administered via the objective using the CoolLED pE-4000 from CoolLED Ltd for the whoele duration of each -120 mV pulse (1.8 s) of the repetitive stimulation protocol. The spectral output at 365 nm and 470 nm declared by the manufacturer is shown in supplementary Figure 6B. The LED intensity was adjusted to 23.5 mW (15% of the maximum LED

power) for UV light and 11.8 mW (9% of the maximum LED power) for blue light. These light pulses were transmitted through the 40x objective lens.

Slice experiments were performed in accordance with the guidelines of the Swiss Federal Act on Animal Protection and Swiss Animal Protection Ordinance. Experiments were approved by the ethics committee of the University of Geneva and the Cantonal Veterinary Office (license GE/121/19).

In vitro plasma stability assay

Human plasma was melted gradually at room temperature before using. 10 mL of stock solution of **1b** (40 mM) was added to 390 mL of human plasma and the mixture was vortexed and incubated at 37 °C for 24 hours. The experiment was performed in duplicate. At specific time points, a 50 mL portion was removed from the mixture under incubation and added to 150 mL of cold acetonitrile to precipitate the proteins. The sample was centrifugated at 4°C for 10 min at 14.000 rpm, filtered, and analysed by HPLC/UV.

Maintenance of zebrafish and drug injection

Wild-type zebrafish (RIKEN WT) were obtained from the Riken BioResource Research Center (Saitama, Japan) and maintained in water at 28 °C with a 14-hour light cycle (8:00–22:00) and 10-hour darkness (22:00–8:00). Before spawning, male and female fish were placed in a mating tank separated by a partition, which was removed on the spawning day. Eggs were promptly collected into a 10 cm dish filled with egg water (0.006% sea salt and 0.01% methylene blue) immediately after spawning.

1a and **1b** were dissolved in DMSO, and stock solutions of 1 M concentration were prepared and stored at −20 °C. On the day of the experiment, the stock solution was diluted with distilled water to a concentration of 1 mM. Zebrafish larvae at 48 hpf (hours post-fertilization) were anesthetized with 0.01% tricaine and injected into the pericardial region with approximately 1-2 nL of 1 mM **1a** or **1b** or vehicle (0.1% DMSO), with an estimated final concentration of 100 μM. Injection was performed under red light to avoid possible degradation of **1a** or **1b**.

All experimental protocols were approved by the Institutional Animal Care and Use Committees at Jichi Medical University.

Heart rate measurement

After the injection into the pericardial region, the zebrafish heart was illuminated with a mercury lamp with filters for UV (U-MWU2; 330-385 nm for excitation) or CFP (U-MCFPHQ; 425-445 nm for excitation) under an MVX10 microscope (Olympus). The spectra of the excitation filters are reported in Figure 6C. Zebrafish were anesthetized with 0.01% tricaine. The peak wavelength and power with the UV and CFP filters were 365 nm (0.5 mW/mm^2) and 436 nm (2 mW/mm^2), respectively. The heart was illuminated for 2 minutes with UV and 10 minutes with blue light. Movies were taken with a Zyla sCMOS camera (Andor Technology, Belfast) at room temperature. The video was imported into ImageJ software and heart rates at each time point were determined from the average of 10 intervals of contraction events around that time. All heart rate measurements were done within 60 min after the injection.

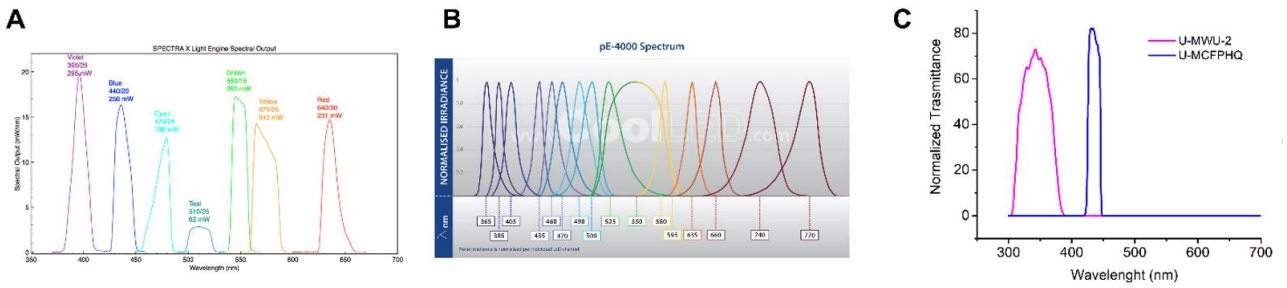

Figure 6: Light sources spectra used for experiments in HEK293T cells (A) and neuron brain slices (B). Spectra of the excitation filters used in zebrafish experiments (C).

ASSOCIATED CONTENT

Supporting Information. The Supporting Information is available free of charge on the …

^{1}H NMR, ^{13}C NMR, HRMS and UV-Vis and emission spectra of **1a** and **1b**; HPLC chromatograms of **1a**, **1b** and ivabradine. Determination of the solubility of **1a** and **1b** in aqueous buffer. Photophysical and photochemical characterization of **1a** and **1b**. *In vitro* cytotoxicity assay. (PDF)

SMILES (CSV)

AUTHOR INFORMATION

Corresponding Authors

Cristiano Bolchi - Dipartimento di Scienze Farmaceutiche, Università degli Studi di Milano, via Mangiagalli 25, I-20133 Milano, Italy; orcid.org/0000-0002-6726-9501; Phone: +390250319347. E-mail: cristiano.bolchi@unimi.it

Anna Moroni – Dipartimento di Bioscienze and CNR IBF-Mi, Università degli Studi di Milano, via Giovanni Celoria 26, I-20133 Milano, Italy; orcid.org/0000-0002-1860-406X; Phone: +390250314826. E-mail: anna.moroni@unimi.it

Authors

Alessandro Porro – *Department of Biosciences, Università degli Studi of Milan, I-20133 Milano, Italy*; e-mail: alessandro.porro2@unimi.it

Edoardo Armano – *Department of Pharmaceutical Sciences, Università degli Studi of Milan, I-20133 Milano, Italy*; e-mail: edoardo.armano@unimi.it

Federico Brandalise – *Department of Biosciences, Università degli Studi of Milan, I-20133 Milano, Italy;* orcid.org/0000-0002-2033-5719; e-mail: federico.brandalise@unimi.it

Rebecca Appiani – *Department of Pharmaceutical Sciences, Università degli Studi of Milan, I-20133 Milano, Italy*

Monica Beltrame – *Department of Biosciences, Università degli Studi of Milan, I-20133 Milano, Italy;* orcid.org/0000-0001-5094-3494; e-mail: monica.beltrame@unimi.it

Andrea Saponaro – *Department of Pharmacological and Biomolecular Sciences, Università degli Studi of Milan, I-20133 Milano, Italy*

Clelia Dallanoce - *Department of Pharmaceutical Sciences, Università degli Studi of Milan, I-20133 Milano, Italy;* e-mail: clelia.dallanoce@unimi.it

Koichi Nakajo – *Division of Integrative Physiology, Department of Physiology, Jichi Medical University, Kawachi District, 329-0498 Japan*; e-mail: knakajo@jichi.ac.jp

Kaei Ryu – *Division of Integrative Physiology, Department of Physiology, Jichi Medical University, Kawachi District, 329-0498 Japan;* e-mail: d2309@jichi.ac.jp

Roberta Leone – *Department of Biosciences, Università degli Studi of Milan, I-20133 Milano, Italy;* e-mail: roby.leone88@gmail.com

Gerhard Thiel – *Department of Biology, TU-Darmstadt, 64287 Darmstadt, Germany;* e-mail: thiel@bio.tu-darmstadt.de

Marco Pallavicini - *Department of Pharmaceutical Sciences, Università degli Studi of Milan, I-20133 Milano, Italy;* e-mail: marco.pallavicini@unimi.it

Author Contributions

A.P. and E.A. are equally contributing first authors.

Funding Sources

Fondazione Telethon grant GGP20021 to Anna Moroni, Università degli Studi di Milano grant SEED 2019 1177 to Cristiano Bolchi and Andrea Saponaro

ABBREVIATIONS USED

BHQ, 8-bromo-7-hydroxy-2-quinolinylmethyl; BHQ-IVA, BHQ protected ivabradine; BHQ-OH 8-bromo-7-hydroxy-2-hydroxymethylquinoline; IVA, ivabradine.

References

(1) Robinson, R. B.; Siegelbaum, S. A. Hyperpolarization-activated cation currents: from molecules to physiological function. *Annu. Rev. Physiol.* **2003**, *65*, 453-480.

(2) Rivolta, I.; Binda, A.; Masi, A.; DiFrancesco, J. C. Cardiac and neuronal HCN channelopaties. *Pflugers Arch.* **2020**, *472*, 931-951.

(3) Santoro, B.; Shah, M. M. Hyperpolarization-activated cyclic nucleotide gated channels as drug targets for neurological disorders. *Annu. Rev. Pharmacol. Toxicol.* **2020**, *60*, 109-131.

(4) Harde, E.; Hierl, M.; Weber, M.; Waiz, D.; Wyler, R.; Wach, J. Y.; Haab, R.; Gundfinger, A.; He, W.; Schnider, P.; Paina, M.; Rolland, J. F.; Greiter-Wilke, A.; Gasser, R.; Reutlinger, M.; Dupont, A.; Roberts, S.; O'Connor, E. C.; Bertels, B.; Hall, B. J. Selective and brain-penetrant HCN1 inhibitors reveal links between synaptic integration, cortical function, and working memory. *Cell. Chem. Biol.* **2024**, *31*, 577-592.

(5) Emery, E. C.; Young, G. T.; Berrocoso, E. M.; Chen, L.; McNaughton, P. A. HCN2 ion channels play a central role in inflammatory and neuropathic pain. *Science* **2011**, *333*, 1462-1466.

(6) Young, G. T.; Emery, E. C.; Mooney, E. R.; Tsantoulas, C.; McNaughton, P. A. Inflammatory and neuropathic pain are rapidly suppressed by peripheral block of hyperpolarization-activated cyclic nucleotide-gated ion channels. *Pain* **2014**, *155*, 1708-1719.

(7) Rushworth, G. F.; Lambrakis, P.; Leslie, S. J. Ivabradine: a new rate-limiting therapy of coronary artery disease and heart failure. *Ther. Adv. Drug Saf.* **2011**, *2*, 19-28.

(8) Scicchitano, S.; Cortese, F.; Ricci, G.; Carbonara, S.; Moncelli, M.; Iacoviello, M.; Cecere, A.; Gesualdo, M.; Zito, A.; Caldarola, P.; Scrutinio, D.; Lagioia, R.; Riccioni, G.; Ciccone, M. M. Ivabradine, coronary artery disease, and heart failure: beyond rhtthm control. *Drug Des. Dev. Ther.* **2014**, *8*, 689-700.

(9) Bucchi, A.; Tognati, A.; Milanesi, R.; Baruscotti, M.; DiFrancesco, D. Properties of ivabradine-induced block of HCN1 and HCN4 pacemaker channels. *J. Physiol.* **2006**, *572*, 335-346.

(10) Saponaro, A.; Krumbach, J. H.; Chaves-Sanjuan, A.; Sharifzadeh, S. A.; Porro, A.; Castelli, R.; Hamacher, K.; Bolognesi, M.; DiFrancesco, D.; Clarke, O.; Thiel, G.; Moroni, A. Structural determinants of ivabradine block of the open pore of HCN4. *PNAS* **2024**, *121*, e2402259121.

(11) Romanelli, M. N.; Sartiani, L.; Masi, A.; Mannaioni, G.; Manetti, D.; Mugelli, A.; Cerbai, E. HCN channels modulators: the need for selectivity. *Curr. Top. Med. Chem.* **20016**, *16*, 1764-1791.

(12) Balducci, V.; Credi, C.; Sacconi, L.; Romanelli, M. N.; Sartiani, L.; Cerbai, E. The HCN channel as a pharmaological target: Why, where, and how to block it. *Prog. Biphys. Mol. Biol.* **2021**, *166*, 173-181.

(13) Ankenbruck, N.; Courtney, T.; Naro, Y.; Deiters, A. Optochemical control of biological processes in cells and animals. *Angew. Chem., Int. Ed.* **2018**, *57*, 2768-2798.

(14) Silva, J. M.; Silva, E.; Reis, R. L. Light-triggered release of photocaged therapeutics – Where are we now? *J. Controlled Release* **2019**, *298*, 154-176.

(15) Zhu, W. F.; Empel, C.; Pelliccia, S.; Koenigs, R. M.; Proschak, E.; Hernandez-Olmos, V. Photochemistry in medicinal chemistry and chemical biology. *J. Med. Chem.* **2024**, *67*, 4322-4345.

(16) Hansen, M. J.; Velema, W. A.; Lerch, M. M.; Szymanski, W.; Feringa, B. L. Wavelength-selective cleavage of photoprotecting groups: strategies and applications in dynamic systems. *Chem. Soc. Rev.* **2015**, *44*, 3358-3377.

(17) Ellis-Davies, G. C. R. Reverse engineering caged compounds: design principles for their application in biology. *Angew. Chem., Int. Ed.* **2023**, *62*, e202206083.

(18) Cannon, J.; Tang, S.; Choi, S. K. Caged oxime reactivators designed for the light control of acetylcholinesterase reactivation. *Photochem. Photobiol.* **2022**, *98*, 334-346.

(19) Inlay, M. A.; Choe, V.; Bharathi, S.; Fernhoff, N. B.; Baker Jr, J. R.; Weissman, I. L.; Choi, S. K. Synthesis of a photocaged tamoxifen for light-dependent activation of Cre-Er recombinase-driven gene modification. *Chem. Commun.* **2013**, *49*, 4971-4973.

(20) Bownik, I.; Šebej, P.; Literák, J.; Heger, D.; Šimek, Z.; Givens, R. S.; Klán, P. 4-Hydroxyphenacyl ammonium salts: a photoremovable protecting group for amines in aqueous solution *J. Org. Chem.* **2015**, *80*, 9713-9721.

(21) Asad, N.; Deodato, D.; Lan, X.; Widegren, M. B.; Phillips, D. L. Du, L.; Dore, T. Photochemical activation of tertiary amines for applications in study cell physiology. *J. Am. Chem. Soc.* **2017**, *139*, 12591-12600.

(22) Banala, S.; Arvin, M. C.; Bannon, N. M.; Jin, X. T.; Macklin, J. J.; Wang, Y.; peng, C.; Zhao, G.; Marshall, J. J.; Gee, K. R.; Wokosin, D. L.; Kim, V. J.; McIntosh, J. M.; Contractor, A.; Lester, H. A.; Kozorovitskiy, Y.; Drenan, R. M.; Lavis, L. D. Photoactivatable drugs for nicotinic optopharmacology. *Nat. Methods* **2018**, *15*, 347-350.

(23) Ragueneau, I.; Laveille, C.; Jochemsen, R.; Resplandy, G.; Funck-Brentano, C.; Jaillon, P. Pharmacokinetc-pharmacodynamic modelling of the effects of ivabradine, a direct sinus node inhibitor, on heat rate in healthy volunteers. *Clin. Pharmacol. Ther.* **1998**, *64*, 192-203.

(24) Fedoryak, O. D.; Dore, T. M. Brominated hydroxyquinoline as a photolabile protecting group with sensitivity to multiphoton excitation. *Org. Lett.* **2002**, *4*, 3419-3422.

(25) Zhu, Y.; Pavlos, C. M.; Toscano, J. P.; Dore, T. M. 8-Bromo-7-hydroxyquinoline as a photoremovable protecting group for physiological use: mechanism and scope. *J. Am. Chem. Soc.* **2006**, *128*, 4267-4276.

(26) Ma, J.; Rea, A. C.; An, H.; Ma, C.; Guan, X.; Li, M. D.; Su, T.; Yeung, C. S.; Harris, K. T.; Zhu, Y.; Nganga, J. L.; Fedoryak, O. D.; Dore, T. M.; Phillips, D. L. Unraveling the mechanism

of the photodeprotection reaction of 8-bromo- and 8-chloro-7-hydroxyquinoline caged acetates. *Chem. Eur. J.* **2012**, *18*, 6854-6865.

(27) Rea, A. C.; Vandenberg, L. N.; ball, R. E.; Snouffer, A. A.; Hudson, A. G.; Zhu, Y.; McLain, E. D.; Johnston, L. L.; Lauderdale, J. D.; Levin, M.; Dore, T. M. Light-activated serotonin for exploring its action in biological systems. *Che. Biol.* **2013**, *20*, 1536-1546.

(28) McLain, D. E.; Rea, A. C.; Widegren, M. B.; Dore, T. M. Photoactivatable, biologically-relevant phenols with sensitivity toward 2-photon excitation. *Photochem. Photobiol. Sci.* **2015**, *14*, 2151-2158.

(29) Pikul, P.; Jamrogiewicz, M.; Nowakowska, J.; Hewelt-Belka, W.; Ciura, K. Forced degradation stidies of ivabradine and *in silico* toxicology predictions for its new designated imputities. *Front. Pharmacol.* **2016**, *7*, 117.

(30) Liu, J.; Kasuya, G.; Zempo, B.; Nakajo, K. Two HCN4 channels play functional roles in the zebrafish heart. *Front. Physiol.* **2022**, *13*, 901571.

Table of contents graphic